



Article

Fabrication and Characterization of AlGa_N-Based UV LEDs with a ITO/Ga₂O₃/Ag/Ga₂O₃ Transparent Conductive Electrode

Hong Wang^{1,2,3,*} , Quanbin Zhou¹ , Siwei Liang^{1,2} and Rulian Wen^{1,2}

¹ Engineering Research Center for Optoelectronics of Guangdong Province, School of Electronics and Information Engineering, South China University of Technology, Guangzhou 510640, China; zhouquanbin86@163.com (Q.Z.); 201620122572@mail.scut.edu.cn (S.L.); wr1_789@163.com (R.W.)

² School of Physics and Optoelectronics, South China university of Technology, Guangzhou 510640, China

³ Zhongshan Institute of Modern Industrial Technology, South China University of Technology, Zhongshan 528437, China

* Correspondence: phhwang@scut.edu.cn; Tel.: +86-136-0006-6193

Received: 30 November 2018; Accepted: 31 December 2018; Published: 5 January 2019



Abstract: We fabricated a complex transparent conductive electrode (TCE) based on Ga₂O₃ for AlGa_N-based ultraviolet light-emitting diodes. The complex TCE consists of a 10 nm ITO, a 15 nm Ga₂O₃, a 7 nm Ag, and a 15 nm Ga₂O₃, forming a ITO/Ga₂O₃/Ag/Ga₂O₃ multilayer. The metal layer embedded into Ga₂O₃ and the thin ITO contact layer improves current spreading and electrode contact properties. It is found that the ITO/Ga₂O₃/Ag/Ga₂O₃ multilayer can reach a 92.8% transmittance at 365 nm and a specific contact resistance of 10⁻³ Ω·cm² with suitable annealing conditions.

Keywords: transparent conductive electrode; Ga₂O₃; AlGa_N-based ultraviolet light-emitting diode; transmittance; sheet resistance

1. Introduction

AlGa_N-based ultraviolet (UV) light-emitting diodes (LEDs) can achieve the full wavelength coverage of UVA (400–320 nm), UVB (320–280 nm) and UVC (280–200 nm) by changing Al content. As a result, AlGa_N-based UV LEDs have attracted considerable attention and are seen as a promising lighting source for different applications in environmental cleaning, medicine, printing, microscopy and lighting [1–6]. However, the external quantum efficiency (EQE) of AlGa_N-based UV LEDs is still much lower than that of the commercially available blue LEDs with an EQE close to 20% for UVA and <1% for UVC devices [7–9]. This phenomenon obstructs commercial applications of the AlGa_N-based UV LEDs. Indium tin oxide (ITO) is widely used as transparent contact layers in traditional Ga_N-based blue and green LEDs. However, there is serious light absorption in the ITO in the ultraviolet band due to the band gap of ITO ranging from 3.5 eV to 4.3 eV [10,11]. Previous studies reported that doping metals in ITO would reduce the light absorption in near UV LEDs. The transmittance of ITO at wavelengths above 380 nm can reach about 90% by optimizing the thickness of metal and the annealing temperature [12–15]. But the transmittance of ITO still decreases rapidly when the wavelength becomes shorter. Thus, it is very urgent for a layer with higher transmittance in ultraviolet band to be able to replace the traditional ITO transparent conductive electrode (TCE) in UV LEDs.

Ga₂O₃, which has a bandgap from 4.9 eV to 5 eV, is an attractive alternative for TCE in UV LEDs because of its high transmittance in UV band [16–18]. In addition, a large size and high quality Ga₂O₃ thin film can be fabricated by single crystals synthesized by the melt growth method [19]. This material has been studied in the fields of metal semiconductor field effect transistors, metal oxide semiconductor

field effect transistors and Schottky barrier diodes. However, the conductivity of Ga₂O₃ is very poor. Many approaches have been developed to promote the conductivity of Ga₂O₃. Orita Mi Hiramatsu H et al. improved the conductivity of β-Ga₂O₃ by doping In or Sn into Ga₂O₃ [16]. The (201)-oriented Sn-doped β-Ga₂O₃ films obtained a maximum conductivity of 8.2 S/cm (about $1.22 \times 10^4 \Omega/\text{sq}$). But it is still too low to be used as TCE in UV LED. Liu JJ et al. grew ITO thin films in Ga₂O₃ films and improved the sheet resistance and transmittance of Ga₂O₃/ITO films by adjusting the growth temperature and the thickness of ITO [17]. A sheet resistance of 323 Ω/sq and a transmittance at 280 nm of 77.6% can be achieved. Jae-kwan Kim et al. realized that the transmittance at 380 nm is 80.944% and the sheet resistance is 58.6 Ω/sq [20]. The Kie Young Woo group in Korea prepared the Ag/Ga₂O₃ model by learning the ITO/Ag/ITO model [21]. The contact characteristics and conductivity of the Ga₂O₃ films were improved by the Ag intercalation layer, and the transmittance at 380 nm and specific contact resistivity of the Ag/Ga₂O₃ thin film were 91% and $3.06 \times 10^{-2} \Omega \cdot \text{cm}^2$ respectively.

In this paper, a complex TCE based on Ga₂O₃ is proposed to enhance the efficiency of UV LEDs. We prepared the complex Ga₂O₃-based TCE by depositing an ITO contact layer, a Ga₂O₃ layer, an Ag metal intercalation layer and another Ga₂O₃ layer in sequence, forming an ITO/Ga₂O₃/Ag/Ga₂O₃ multilayer. The resistance and transmittance ITO/Ga₂O₃/Ag/Ga₂O₃ multilayer with a different annealing temperature were studied and analyzed systematically. The sheet resistance of the ITO/Ga₂O₃/Ag/Ga₂O₃ multilayer was detected by four-point probe methods. The optical transmittance was measured by a UV/visible spectrophotometer. The surface roughness of these ITO/Ga₂O₃/Ag/Ga₂O₃ multilayer were measured by atomic force microscope (AFM). The X-ray photoelectron spectroscopy (XPS) and Auger electron spectroscopy (AES) measurements were also used to analyze the ITO/Ga₂O₃/Ag/Ga₂O₃ multilayer. Furthermore, we employed the ITO/Ga₂O₃/Ag/Ga₂O₃ multilayer as TCEs on 365 nm UV epitaxy in comparison to those with conventional ITO.

2. Materials and Methods

To investigate the influence of a Ag intercalation layer on the Ga₂O₃ layer, a Ga₂O₃/Ag/Ga₂O₃ (15 nm/7 nm/15 nm) multilayer was deposited on quartz substrates and then annealed at different conditions. The quartz substrates were first washed in acetone, isopropanol and deionized water and dried by nitrogen. After that, Ga₂O₃, Ag and Ga₂O₃ were sequentially deposited on the quartz substrates in magnetron sputtering equipment. In order to reduce the resistivity of the Ga₂O₃ layer but not affect its transmittance, the thickness of the Ag embedding interlayer and Ga₂O₃ were set to be 7 nm and 15 nm respectively. The Ga₂O₃ thin films were all deposited by RF magnetron sputtering of Ga₂O₃ (purity 99.99%) ceramic target, and the Ag thin film was deposited by direct current magnetron sputtering of the Ag target. The sputtering cavity was pumped to 5×10^{-6} Pa before the sputtering begin. The sputtering atmosphere was pure argon with the pressure of 5 mtorr. The rotation speed of the cavity substrate is 20 rpm. The temperature was controlled at about $35 \text{ }^\circ\text{C} \pm 1 \text{ }^\circ\text{C}$ by feedback control heater during deposition. Afterwards, all the Ga₂O₃/Ag/Ga₂O₃ multilayer samples were annealed by a rapid thermal annealing (RTA) system at a different temperature and ambient. We used X-ray photoelectron spectroscopy (XPS) and Auger electron spectroscopy (AES) to analyze the element diffusion effect of the Ga₂O₃/Ag/Ga₂O₃ multilayer.

To further improve the contact between Ga₂O₃ and AlGaIn-based UV epitaxy, we insert an ITO thin film below the Ga₂O₃/Ag/Ga₂O₃ multilayer as a contact layer. We prepared ITO/Ga₂O₃/Ag/Ga₂O₃ multilayer on quartz substrates. Before the deposition of Ga₂O₃/Ag/Ga₂O₃ multilayer, a 10 nm ITO was deposited on quartz substrates by RF magnetron sputtering of ITO (In₂O₃: 90 wt%, SnO₂: 10 wt%) and then annealed by RTA. Subsequently, Ga₂O₃/Ag/Ga₂O₃ multilayer was deposited on the annealed ITO thin films and the whole ITO/Ga₂O₃/Ag/Ga₂O₃ multilayer was annealed again.

Finally, we prepared ITO/Ga₂O₃/Ag/Ga₂O₃ multilayer on AlGaIn-based UV epitaxy in the same method to study the specific contact resistance through the CTLM model. A 47 nm ITO thin film on quartz substrates and epitaxy was also prepared as reference, which was annealed at 600 °C for

1 min in a mixture of N_2/O_2 (200 sccm:35 sccm) ambient. The procedures of ITO/ Ga_2O_3 /Ag/ Ga_2O_3 multilayer and optical micrograph of contact surface on CTLM patterns are shown in Figure 1.

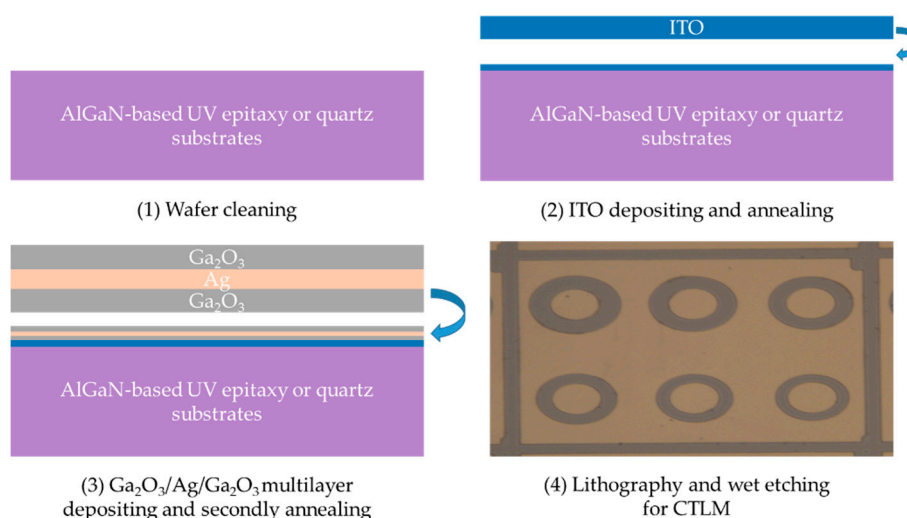


Figure 1. The procedures of ITO/ Ga_2O_3 /Ag/ Ga_2O_3 multilayer and optical micrograph of contact surface on CTLM patterns.

3. Results

In order to study the influence of annealing conditions on the sheet resistance of Ga_2O_3 /Ag/ Ga_2O_3 multilayer, a series of Ga_2O_3 /Ag/ Ga_2O_3 multilayer on quartz substrates were annealed at different temperature and ambient. The annealing temperature changed from 400 °C to 600 °C with the annealing ambient changing from N_2/O_2 mixture and pure O_2 ambient. As shown in Table 1, the sheet resistance increases with the decrease of annealing temperature. It is found that the Ga_2O_3 /Ag/ Ga_2O_3 multilayer could reach the lowest sheet resistance of 16.45 Ω /sq after being annealed at 600 °C for 1 min in an N_2/O_2 mixture ambient. The result means that the effect of Ag as the insertion layer is not obvious at low temperature, and the metal diffusion reaction is not sufficient. The metal insertion layer in the film can fully diffuse to the Ga_2O_3 layer and decrease the resistance value of the Ga_2O_3 /Ag/ Ga_2O_3 multilayer when the temperature reaches 600 °C. The resistance of the multilayer annealed at 600 °C in pure oxygen ambient is higher than that of the multilayer in an N_2/O_2 mixture annealing ambient. Besides, the higher the oxygen ratio in the annealing atmosphere, the higher the multilayer resistance value becomes. The reason for this is that metal oxides form and then affect the resistance of film [22,23].

Table 1. Sheet resistance of a Ga_2O_3 /Ag/ Ga_2O_3 multilayer on quartz substrates at different annealing conditions.

No.	Annealing Temperature	Annealing Ambient	Annealing Time	Sheet Resistance (Ω /sq)
1	As deposited	As deposited	As deposited	23.86
2	400 °C	N_2 200 sccm: O_2 35 sccm	1 min	32.1
3	500 °C	N_2 200 sccm: O_2 35 sccm	1 min	27.74
4	600 °C	N_2 200 sccm: O_2 35 sccm	1 min	16.45
5	600 °C	O_2 35 sccm	3 min	30.6
6	600 °C	O_2 100 sccm	1 min	40.93

Figure 2 and Table 2 show the XPS energy spectral of Ga_2O_3 /Ag/ Ga_2O_3 multilayer on quartz substrate before and after annealing at 600 °C for 1 min in N_2/O_2 mixture ambient. The energy intensity, peak value quantum-number vertex, high half-width and atomic fraction content of Ag3d, O1s, Ga2p₃ were measured at the depth of about 10 nm of the multilayer. The open symbol and solid symbol in Figure 2 represent the energy intensity of the elements before and after annealing

respectively. We can see that the energy value of element Ag3d is high, the quantum number per second is 13581 states/s, and the atomic fraction is 0.47 before annealing. After annealing, the energy intensity and the atomic ratio of Ag atom decrease relatively, which is 6651.8 counts/s and 0.29%, respectively. The energy and atomic ratio of Ga and O increase a little after annealing. The decrease of atomic ratio of Ag atom means that the process of annealing results in diffusion of Ag in the multilayer. Therefore, the sheet resistance of annealed Ga₂O₃/Ag/Ga₂O₃ multilayer decreases compared to that of the as-deposited sample due to the diffusion of internal elements.

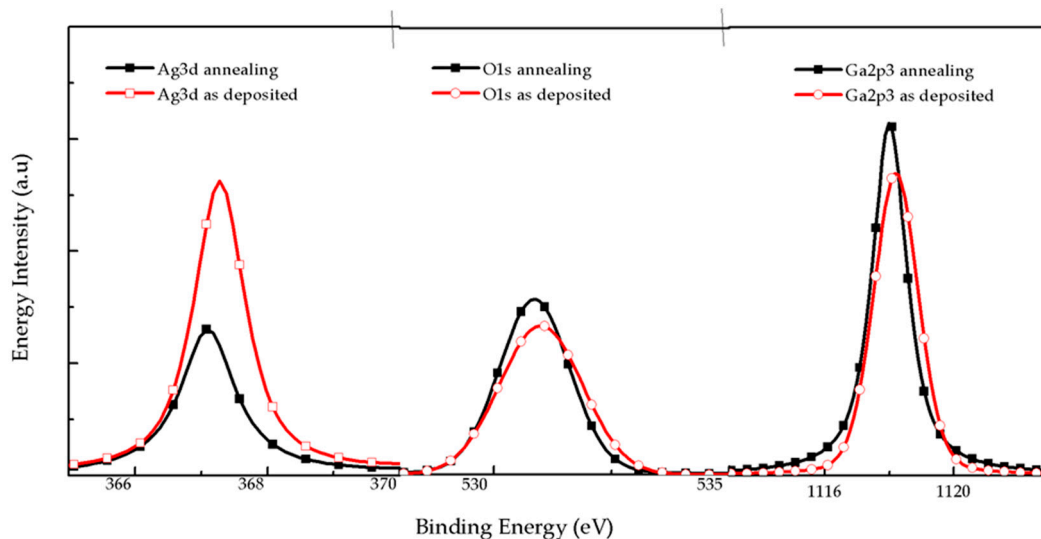


Figure 2. XPS spectrum for Ag3d, O1s and Ga2p₃ of Ga₂O₃/Ag/Ga₂O₃ multilayer on quartz substrates.

Table 2. XPS data of Ga₂O₃/Ag/Ga₂O₃ multilayer on quartz substrates.

Name	As Deposited	Annealing	As Deposited	Annealing	As Deposited	Annealing	As Deposited	Annealing
	Peak BE		Height CPS		FWHM eV		Atomic %	
Ag3d	367.24	367.06	13,581.03	6651.81	0.95	0.95	0.47	0.29
O1s	530.89	530.7	224,669.16	265,423	2.04	1.7	50.67	50.97
Ga2p ₃	1118.21	1117.93	705,296.57	772,390.77	1.66	1.62	34.31	35.62

In addition, to further identify the distribution of composition in Ga₂O₃/Ag/Ga₂O₃ multilayer, we analyzed the Ga₂O₃/Ag/Ga₂O₃ multilayer on quartz substrate using AES measurement. Figure 3 shows the AES depth profiles of the Ga₂O₃/Ag/Ga₂O₃ multilayer before and after annealing at 600 °C for 1 min in N₂/O₂ mixture ambient. For the multilayer before annealing, the atomic percent of Ag is low in the surface and increases after a specific sputter time, which means that the Ag do not diffuse into the multilayer. Since the Ga₂O₃ and quartz substrates have poor conductivity, the atomic percent will become random and fluctuant due to the charge accumulation effect when the sputter time increases. By contrast, the atomic percent of Ag increases at the beginning of sputtering and the Ag atoms distribute more evenly in the whole multilayer after annealing as shown in Figure 3b. This result demonstrates that the Ag will diffuses into the Ga₂O₃ layer during the annealing process, leading to the reduction of sheet resistance of the Ga₂O₃/Ag/Ga₂O₃ multilayer.

Because of the bad contact property between Ga₂O₃ and p-GaN on epitaxial wafer, we insert a 10 nm ITO thin film below Ga₂O₃ as the contact layer. In order to optimal the transmittance and sheet resistance of the ITO/Ga₂O₃/Ag/Ga₂O₃ multilayer, we prepared five ITO/Ga₂O₃/Ag/Ga₂O₃ multilayer samples on quartz substrates and changed the annealing temperature as shown in Table 3. Among the five samples, sample 1 was not annealed. Sample 2 was annealed at 600 °C as a whole. For sample 3 to sample 5, the 10 nm ITO layer was firstly annealed at 550/600/650 °C respectively and then the whole ITO/Ga₂O₃/Ag/Ga₂O₃ multilayer were annealed at 600 °C. The annealing process of ITO and ITO/Ga₂O₃/Ag/Ga₂O₃ multilayer both maintained in N₂/O₂ (200 sccm:35 sccm) mixture

ambient for 1 min. Figure 4 is the transmittance curves of five samples at range of 300 nm to 450 nm. It is obvious that sample 4, which was annealed at 600 °C at first and then at 600 °C again, has the highest transmittance of 92.68% at 365 nm and the lowest sheet resistance of 20.1 Ω/sq.

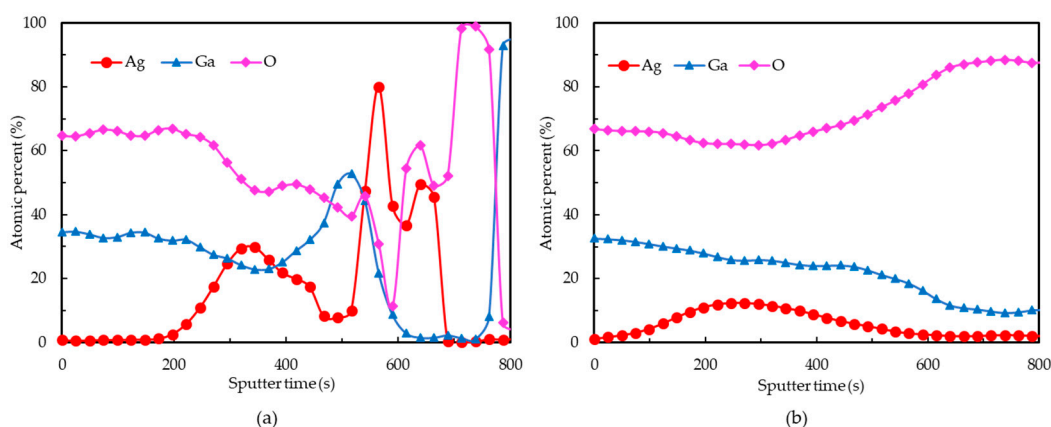


Figure 3. AES depth profiles of the Ga₂O₃/Ag/Ga₂O₃ multilayer on quartz substrates (a) before annealing and (b) after annealing.

Table 3. The transmittance and sheet resistance of ITO/Ga₂O₃/Ag/Ga₂O₃ multilayer on quartz substrates.

Sample	Annealing Temperature		Sheet Resistance	Transmittance at 365 nm
	10 nm ITO	ITO/Ga ₂ O ₃ /Ag/Ga ₂ O ₃		
1	No annealing	No annealing	386.7 Ω/sq	48.04%
2	No annealing	600 °C	164.0 Ω/sq	69.35%
3	550 °C		36.9 Ω/sq	80.31%
4	600 °C		20.1 Ω/sq	92.68%
5	650 °C		48.1 Ω/sq	72.09%

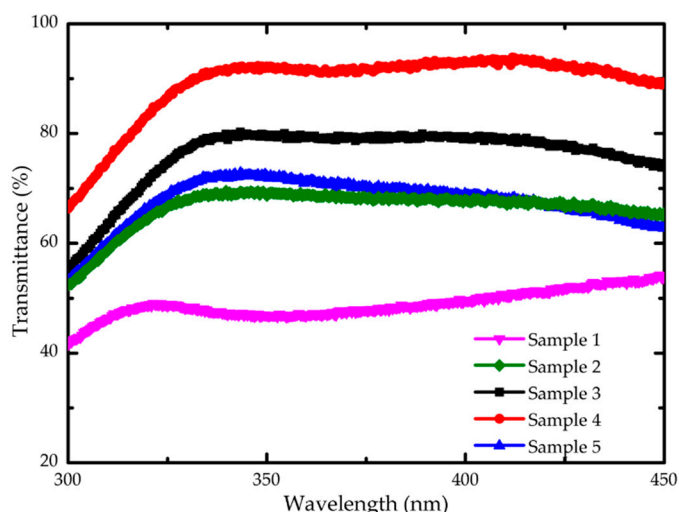


Figure 4. The transmittance curves of ITO/Ga₂O₃/Ag/Ga₂O₃ multilayer on quartz substrates after annealing.

In addition, we compared the transmittance and sheet resistance of sample 4 and a 47 nm ITO thin film on quartz substrate. The 47 nm ITO sample was annealed at 600 °C in N₂/O₂ (200 sccm:35 sccm) mixture ambient for 1 min. Figure 5a plots the transmittance curves of sample 4 and 47 nm ITO.

The ITO/Ga₂O₃/Ag/Ga₂O₃ multilayer demonstrates better transmittance property than 47 nm ITO especially in UV range. To further understand the origin of this result, the optical bandgap Energy E_g of sample 4 and 47 nm ITO was calculated. The E_g can be extracted from the relation between $(\alpha hv)^2$ and hv according to the Equations (1) and (2), as follow:

$$\alpha hv = C(hv - E_g)^{1/2} \quad (1)$$

$$hv = \frac{hc}{\lambda_i} \quad (2)$$

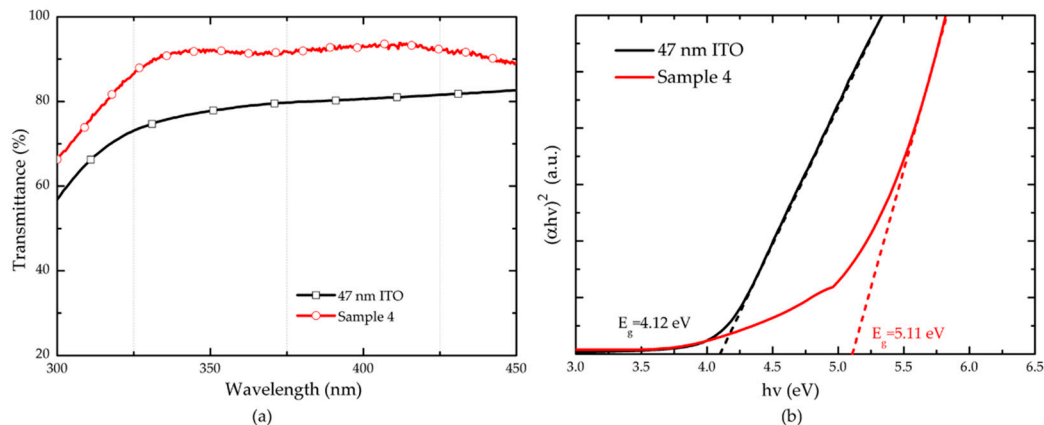


Figure 5. (a) Transmittance and (b) Energy bandgap of sample 4 and 47 nm ITO on quartz substrates.

The E_g can be obtained by extrapolating the linear $(\alpha hv)^2$ versus hv plots to the horizontal axis [24,25]. In Equations (1) and (2), C is a constant of direct transition, α is the light absorption coefficient, hv is the photon energy, h is Planck constant bright, c is the light speed, and λ_i is the wavelength [24,26,27].

If the transmittance T at each λ_i is known, the value of α at each λ_i can be obtained by Equations (3) and (4), as follow:

$$T = \exp(-\alpha d) \quad (3)$$

$$\alpha = \frac{\text{Ln}\left(\frac{1}{T}\right)}{d} \quad (4)$$

where d is the thickness of films. Since we have measured the transmittance T of sample 4 and 47 nm ITO, the curves of $(\alpha hv)^2$ as a function of hv can be obtained as shown in Figure 5b. The optical Energy bandgap E_g of sample 4 is determined to be 4.12 eV, and that of ITO layer is 5.11 eV, by extrapolating the linear section of $(\alpha hv)^2$ to the hv axis. The large band gap means that the absorption of ITO/Ga₂O₃/Ag/Ga₂O₃ multilayer in UV range is smaller than that of 47 nm ITO layer. Table 4 shows the transmittance at 365 nm and sheet resistance of sample 4 and 47 nm ITO. The sample 4 has a reduction in sheet resistance compared to the 47 nm ITO sample. The transmittance of sample 4 is higher than that of 47 nm ITO and other reported metal-doped ITO [12–15]. These results reveal that the ITO/Ga₂O₃/Ag/Ga₂O₃ multilayer exhibits an advantage of transmittance at UV range and conductivity.

Table 4. Transmittance at 365 nm and sheet resistance of sample 4 and 47 nm ITO on quartz substrates.

Sample	47 nm ITO	Sample 4
Transmittance at 365 nm	79.15%	92.68%
Sheet resistance	57.63 Ω/sq	20.1 Ω/sq

Finally, we prepared a series of ITO/Ga₂O₃/Ag/Ga₂O₃ multilayers on AlGa_N-based UV epitaxy to study the specific contact resistance through the CTLM model. These samples were fabricated in the same process as sample 1 and sample 3, 4, 5. The 10 nm ITO contact layer was annealed at 550/600/650 °C respectively, and then the whole ITO/Ga₂O₃/Ag/Ga₂O₃ multilayer was annealed at 600 °C. The annealing process of ITO and the ITO/Ga₂O₃/Ag/Ga₂O₃ multilayer both maintained in N₂/O₂ (200 sccm:35 sccm) mixture ambient for 1 min. As reference, a 47 nm ITO was also deposited on epitaxy and annealed at 600 °C in N₂/O₂ (200 sccm:35 sccm) mixture ambient for 1 min. Figure 6 shows the Ohmic contact characteristics of annealed ITO/Ga₂O₃/Ag/Ga₂O₃ multilayer with p-GaN measured by Electroluminescence system and CTLM mode. The I–V characteristics of the as-deposited ITO/Ga₂O₃/Ag/Ga₂O₃ multilayer are insulated, because the Ga₂O₃ films have the properties of non-diffusion of metals, poor conductivity and insulation on the p-GaN surface. However, the multilayer whose ITO was annealed in nitrogen-oxygen atmosphere at 550 °C /600 °C /650 °C shows linear I–V characteristics on the surface of p-GaN. Also, all the annealed ITO/Ga₂O₃/Ag/Ga₂O₃ multilayers exhibit higher current compared to the 47 nm ITO on p-GaN. The slope of 600 °C annealed I–V curve is highest. The specific contact resistance of 600 °C annealed sample could reach $2.36 \times 10^{-3} \Omega \cdot \text{cm}^2$. In contrast, the specific contact resistance of 47 nm ITO on AlGa_N-based UV epitaxy is $5.68 \times 10^{-3} \Omega \cdot \text{cm}^2$.

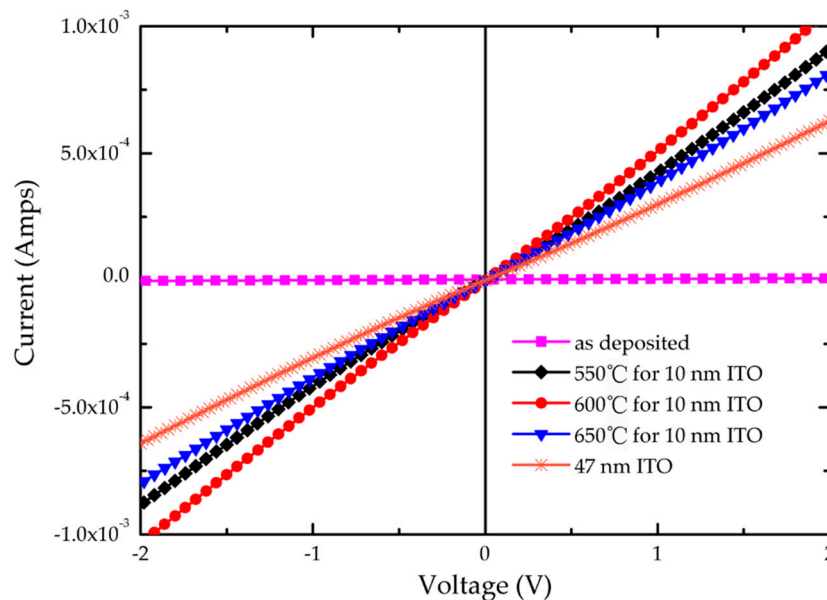


Figure 6. Ohmic contact characteristics of ITO/Ga₂O₃/Ag/Ga₂O₃ multilayer with different annealing temperature for ITO contact layer.

To further compare the differences between ITO/Ga₂O₃/Ag/Ga₂O₃ multilayer and the 47 nm ITO, we measured the surface morphology using scanning electron microscope (SEM) and AFM. The Figure 7a,b show SEM micrographs of the ITO/Ga₂O₃/Ag/Ga₂O₃ multilayer and 47 nm ITO on the AlGa_N-based UV epitaxy. The surface of 47 nm ITO is smoother than that of the ITO/Ga₂O₃/Ag/Ga₂O₃ multilayer. Besides, the thickness of the multilayer is about 48 nm measured by SEM cross-section micrograph. The root-mean-square (RMS) surface roughness of the ITO/Ga₂O₃/Ag/Ga₂O₃ multilayer and 47 nm ITO on a $10 \times 10 \mu\text{m}^2$ area are 6.92 nm and 2.36 nm respectively measured by AFM. A rough surface is beneficial for light emitting from chips to external. The rougher surface of the ITO/Ga₂O₃/Ag/Ga₂O₃ multilayer may be another reason for its higher transmittance.

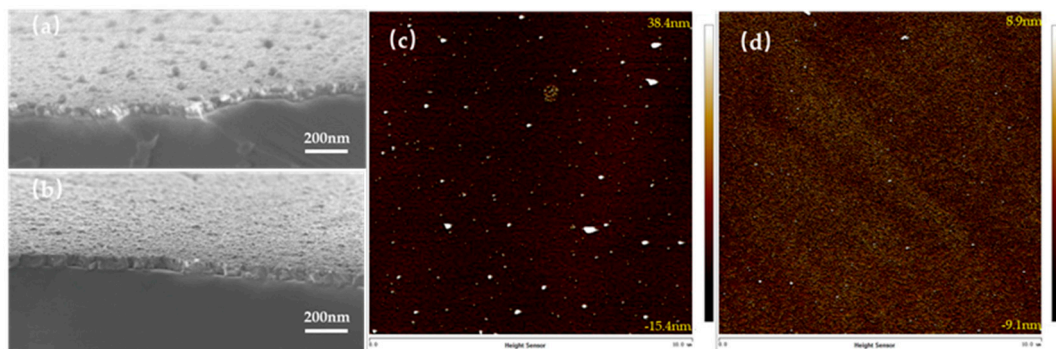


Figure 7. The surface morphology measured by SEM and AFM. (a,c) are for ITO/Ga₂O₃/Ag/Ga₂O₃ multilayer on AlGaN-based UV epitaxy after annealing at 600 °C. (b,d) are for 47 nm ITO on AlGaN-based UV epitaxy after annealing at 600 °C.

4. Conclusions

In this paper, a complex transparent conductive electrode based on Ga₂O₃ for AlGaN-based UV LEDs is proposed. The complex transparent conductive electrode consists of a 10 nm ITO, a 15 nm Ga₂O₃, a 7 nm Ag, and a 15 nm Ga₂O₃, forming a ITO/Ga₂O₃/Ag/Ga₂O₃ multilayer. The ITO/Ga₂O₃/Ag/Ga₂O₃ multilayer was grown by magnetron sputtering. The resistance and transmittance ITO/Ga₂O₃/Ag/Ga₂O₃ multilayer with a different annealing temperature was studied and analyzed systematically. With suitable annealing conditions, the ITO/Ga₂O₃/Ag/Ga₂O₃ multilayer reaches a 92.8% transmittance at 365 nm and a specific contact resistance of $2.36 \times 10^{-3} \Omega \cdot \text{cm}^2$. The XPS and AES results show that the diffusion of Ag in the multilayer leads to a low sheet resistance of the ITO/Ga₂O₃/Ag/Ga₂O₃ multilayer. The reason for the high transmittance of the ITO/Ga₂O₃/Ag/Ga₂O₃ multilayer in the UV range is the 5.11 eV band gap. These situations provide the improvement in optical characteristics of 365 nm UV LEDs. These results indicate that the proposed ITO/Ga₂O₃/Ag/Ga₂O₃ multilayer is a promising alternative for TCE to further improve the optical and electrical performances of AlGaN-based UV LED.

Author Contributions: These authors contributed equally.

Funding: This work was supported by Science and Technologies plan Projects of Guangdong Province (Nos. 2017B010112003, 2017A050506013), and by Applied Technologies Research and Development Projects of Guangdong Province (Nos. 2015B010127013, 2016B010123004), and by Science and Technologies plan Projects of Guangzhou City (Nos. 201504291502518, 201604046021, 201704030139), and by Science and Technology Development Special Fund Projects of Zhongshan City (Nos. 2017F2FC0002, 2017A1009).

Conflicts of Interest: The authors declare no conflict of interest.

References

- Maitland, J. UV curing of inks and coatings in digital printing applications. In Proceedings of the NIP & Digital Fabrication Conference, Baltimore, MD, USA, 18–23 September 2005.
- Yu, C.C.; Chuah, E.C.; Ng, Y.T.; Seah, Y.S.; Tan, P.P.; Chiu, T.H.; Hsieh, T.T. Neonatal status in cesarean section under epidural anesthesia with supplementary oxygen. *Ma Zui Xue Za Zhi = Anaesthesiologica Sinica* **1992**, *30*, 229. [[PubMed](#)]
- Hockberger, P.E. A history of ultraviolet photobiology for humans, animals and microorganisms. *Photochem. Photobiol.* **2010**, *76*, 561–579. [[CrossRef](#)]
- Schreiner, M.; Martínez-Abaigar, J.; Glaab, J.; Jansen, M. Uv-b induced secondary plant metabolites. *Opt. Photonik* **2014**, *9*, 34–37. [[CrossRef](#)]
- Lui, G.Y.; Roser, D.; Corkish, R.; Ashbolt, N.; Jagals, P.; Stuetz, R. Photovoltaic powered ultraviolet and visible light-emitting diodes for sustainable point-of-use disinfection of drinking waters. *Sci. Total Environ.* **2014**, *493*, 185–196. [[CrossRef](#)]
- Hodgkinson, J.; Tatam, R.P. Optical gas sensing: A review. *Meas. Sci. Technol.* **2013**, *24*, 012004. [[CrossRef](#)]

7. Takano, T.; Mino, T.; Sakai, J.; Noguchi, N.; Tsubaki, K.; Hirayama, H. Deep-ultraviolet light-emitting diodes with external quantum efficiency higher than 20% at 275 nm achieved by improving light-extraction efficiency. *Appl. Phys. Express* **2017**, *10*, 031002. [[CrossRef](#)]
8. Inoue, S.; Tamari, N.; Taniguchi, M. 150 mw deep-ultraviolet light-emitting diodes with large-area aln nanophotonic light-extraction structure emitting at 265 nm. *Appl. Phys. Lett.* **2017**, *110*, 141106. [[CrossRef](#)]
9. Shatalov, M.; Sun, W.; Lunev, A.; Hu, X.; Dobrinsky, A.; Bilenko, Y.; Yang, J.; Shur, M.; Gaska, R.; Moe, C. Algan deep-ultraviolet light-emitting diodes with external quantum efficiency above 10%. *Appl. Phys. Express* **2012**, *5*, 2101. [[CrossRef](#)]
10. Toyota, A.; Nakashima, N.; Sagara, T. Uv–visible transmission–absorption spectral study of au nanoparticles on a modified ito electrode at constant potentials and under potential modulation. *J. Electroanal. Chem.* **2004**, *565*, 335–342. [[CrossRef](#)]
11. Lin, Y.H.; Liu, C.Y. Reflectivity and abnormal absorption at ito/al interface. *J. Electron. Mater.* **2009**, *38*, 108–112. [[CrossRef](#)]
12. Lin, Y.H.; Liu, Y.S.; Liu, C.Y. Light output enhancement of near uv-led by using ti-doped ito transparent conducting layer. *IEEE Photonics Technol. Lett.* **2010**, *22*, 1443–1445. [[CrossRef](#)]
13. Jae Hoon, L.; Kie Young, W.; Kyeong Heon, K.; Hee-Dong, K.; Tae Geun, K. Ito/ag/ito multilayer-based transparent conductive electrodes for ultraviolet light-emitting diodes. *Opt. Lett.* **2013**, *38*, 5055–5058.
14. Kim, M.J.; Kim, T.G. Fabrication of metal-deposited indium tin oxides: Its applications to 385 nm light-emitting diodes. *ACS Appl. Mater. Interfaces* **2016**, *8*, 5453–5457. [[CrossRef](#)] [[PubMed](#)]
15. Xu, J.; Zhang, W.; Peng, M.; Dai, J.; Chen, C. Light-extraction enhancement of gan-based 395 nm flip-chip light-emitting diodes by an al-doped ito transparent conductive electrode. *Opt. Lett.* **2018**, *43*, 2684–2687. [[CrossRef](#)] [[PubMed](#)]
16. Orita, M.; Hiramatsu, H.; Ohta, H.; Hirano, M.; Hosono, H. Preparation of highly conductive, deep ultraviolet transparent β -ga₂o₃ thin film at low deposition temperatures. *Thin Solid Films* **2002**, *411*, 134–139. [[CrossRef](#)]
17. Liu, J.; Yan, J.; Shi, L.; Li, T. Semiconductor materials electrical and optical properties of deep ultraviolet transparent conductive Ga₂O₃/ito films by magnetron sputtering. *J. Semicond.* **2010**, *31*, 5–9.
18. Passlack, M.; Schubert, E.F.; Hobson, W.S.; Hong, M.; Moriya, N.; Chu, S.N.G.; Konstadinidis, K.; Mannaerts, J.P.; Schnoes, M.L.; Zydzik, G.J. Ga₂O₃ films for electronic and optoelectronic applications. *J. Appl. Phys.* **1995**, *77*, 686–693. [[CrossRef](#)]
19. Higashiwaki, M.; Sasaki, K.; Murakami, H.; Kumagai, Y.; Koukitu, A.; Kuramata, A.; Masui, T.; Yamakoshi, S. Recent progress in Ga₂O₃ power devices. *Semicond. Sci. Technol.* **2016**, *31*, 034001. [[CrossRef](#)]
20. Kim, J.K.; Lee, J.M. Electrical and optical properties of near uv transparent conductive ito/Ga₂O₃ multilayer films deposited by rf magnetron sputtering. *Appl. Phys. Lett.* **2016**, *109*, 4166. [[CrossRef](#)]
21. Woo, K.Y.; Lee, J.H.; Kim, K.H.; Kim, S.J.; Kim, T.G. Highly transparent conductive ag/Ga₂O₃ electrode for near-ultraviolet light-emitting diodes. *Phys. Status Solidi* **2015**, *211*, 1760–1763. [[CrossRef](#)]
22. Wang, G.; Liu, H.; Zhao, C.; Yang, B.; Huang, X. Optical and electrical properties of annealed ito films. *Acta scientiarum Naturalium Universitatis Jilinensis* **1999**, *4*, 61–65.
23. Cai, Q.; Cao, C.; Jiang, X.; Song, X.; Sun, Z. Microstructures and stoichiometrics of indium-tin-oxide films. *Zhenkong Kexue Yu Jishu Xuebao/J. Vac. Sci. Technol.* **2007**, *27*, 195–199.
24. He, J.; Sun, L.; Chen, S.; Chen, Y.; Yang, P.; Chu, J. Composition dependence of structure and optical properties of cu₂znsn (s, se) 4 solid solutions: An experimental study. *J. Alloy. Compd.* **2012**, *511*, 129–132. [[CrossRef](#)]
25. Washizu, E.; Yamamoto, A.; Abe, Y.; Kawamura, M.; Sasaki, K. Optical and electrochromic properties of rf reactively sputtered wo₃ films. *Solid State Ionics* **2003**, *165*, 175–180. [[CrossRef](#)]
26. Chandramohan, S.; Kanjilal, A.; Tripathi, J.K.; Sarangi, S.N.; Sathyamoorthy, R.; Som, T. Structural and optical properties of mn-doped cds thin films prepared by ion implantation. *J. Appl. Phys.* **2009**, *105*, 3272. [[CrossRef](#)]
27. Lu, X.; Zhuang, Z.; Peng, Q.; Li, Y. Wurtzite cu₂znsns₄ nanocrystals: A novel quaternary semiconductor. *Chem. Commun.* **2011**, *47*, 3141–3143. [[CrossRef](#)] [[PubMed](#)]

